Experimental Mechanics (2010) 50:473–482
DOI 10.1007/s11340-009-9251-8

Crack Stability of Fracture Specimens used to Test Unidirectional Fiber Reinforced Material

A. Szekrényes

Received: 15 June 2008 / Accepted: 20 April 2009 / Published online: 12 May 2009

Abstract The traditional compliance-based criterion of the crack stability in fracture mechanics states that the stability of the crack propagation in the different specimens under different fracture modes is determined by the derivative of the energy release rate with respect to the crack length. In this work the compliance-based criterion is verified by experiments performed on fracture mechanical systems. The large number of experiments carried out on different (mode-I, mode-II, mixed-mode I/II and mixed-mode II/III) specimens shows that the stability of the crack propagation depends on the derivative of the critical displacement (the displacement at the point of fracture initiation) with respect to the crack length. The experimentally established limits of crack stability were compared to the limits of the traditional criterion and it is shown that in each case they lead to approximately the same restriction considering the stable zone of crack propagation.

Keywords Crack stability · Unidirectional fiber reinforced material · Double-cantilever beam · End-notched flexure · Single-cantilever beam · Interlaminar fracture

Introduction

The crack stability problem is an important issue in the interlaminar fracture tests. The crack stability means an infinitesimal change of displacement is accompanied by a finite change in the crack length. For a certain fracture mechanical configuration it is worth the effort to predict what we could expect during the measurements: stable or unstable crack propagation. In the literature a very large amount of experimental work has been published including mode-I [1, 2], mode-II [3, 4] and mixed-mode I/II [5, 6] configurations. Except for some of them (which mainly investigate the stability of mode-II configurations) each ignores the problem of crack stability. For instance, in the mode-I double-cantilever beam (DCB) [7] specimen the crack propagation is always stable. On the other hand under mode-II the stability problem can limit the length of the initial crack [8], while under mixed-mode I/II (being the combination of the mode-I and mode-II) [9] the instability problem can also take place.

The traditional (compliance-based or energy-based) stability criterion [10, page 38] states that the stability depends on the derivative of the energy release rate (ERR) with respect to the crack length: if it is zero or negative then stable crack propagation can be expected. Otherwise instability may take place. Based on this criterion the limit value of the crack length can be determined for a system of which compliance-crack length relationship is known. For the common mode-II beam-like specimens the limit of the crack length is known. On the contrary, the relevant literature does not contain any information for mixed-mode I/II and II/III cases, where the problem of instability also arises.

In this paper the traditional stability criterion is verified by experimental observations. To this end a large number of tests were performed on unidirectional E-glass/polyester composite including mode-I, mode-II, mixed-mode I/II and II/III tests. For each test the limit of crack stability was calculated by using the traditional criterion and the fact of the instability was tried to be observed during experimental tests. The stability loss was accompanied by a sudden crack jump, and the crack length, where the instability took place was believed to be the stability limit. The limits obtained by the

A. Szekrényes (✉)
Department of Applied Mechanics,
Budapest University of Technology and Economics,
Műegyetem rkp. 5., Building MM,
H-1111 Budapest, Hungary
e-mail: szeki@mm.bme.hu

traditional criterion and the experimental observations were compared to each other. In each case the agreement seemed to be very good. Apart from some minor differences a simple formule based on the experimental data leads essentially to the same restrictions as the traditional stability criterion.

The Traditional Criterion

In accordance with the linear elastic fracture mechanics the definition of the crack driving force in a linear elastic body including a crack is [10, 11]:

$$G_C = \frac{dW}{dA} - \frac{dU}{dA}, \tag{1}$$

where W is the work of external forces, U is the strain energy of the system and A is the area of crack face, equation (1) is called the critical ERR. It is convenient to use the Irwin-Kies expression to determine the ERR in delaminated slender beams [10]:

$$G_C = \frac{P^2}{2b}\frac{dC}{da}, \tag{2}$$

where C is the compliance and P is the applied load required for crack propagation. The crack stability of the system is determined by the derivative of the ERR with respect to the crack length. If dG_C/da is zero or negative then stable crack propagation may be expected [8]:

$$\frac{dG_C}{da} \le 0. \tag{3}$$

Equation (3) can be considered under the fixed load or fixed grip conditions [8]. We consider the latter one as a more realistic condition. Equation (2) can be transformed as ($C=\delta/P$):

$$G_C = \frac{\delta^2}{2bC^2}\frac{dC}{da}, \tag{4}$$

where δ is the critical displacement of the specimen at the point of load application. The derivative of the ERR with respect to the crack length is [8]:

$$\frac{dG_C}{da} = \frac{\delta^2}{2bC^2}\left[\frac{d^2C}{da^2} - \frac{2}{C}\left(\frac{dC}{da}\right)^2\right]. \tag{5}$$

It is seen that the stability analysis requires the determination of the compliance vs. crack length relationship. The $C(a)$ curve could be determined in three ways: analytically, numerically or/and experimentally. The analytical solutions are available only for those systems, which can be considered as beams and plates. The numerical solution requires much work, especially when a three-dimensional model is necessary. Finally, very much work is required for the experiments (specimen manufacturing, preparation, experiments, data reduction, scatter of the data etc.). In the followings some well-known fracture mechanical tests are utilized for the stability analysis, namely: mode-I double-cantilever beam (DCB) [1], mode-II end-notched flexure (ENF) [8], four point bend end-notched flexure (4ENF) [4], end-loaded split (ELS) [1, 2], over-notched flexure (ONF) [12, 13], mixed-mode I/II single-cantilever beam (SCB) [14, 15], single-leg bending (SLB) [16], over-leg bending (OLB) [17] (Fig. 1) and mixed-mode II/III modified split-cantilever beam (MSCB) [18, 19] specimens (Fig. 2). In previous publications the compliance of these configurations has been calculated based on linear beam theories [19, 20].

Some Common Specimen Types

In accordance with equation (5) it is necessary to express the compliance of the system. The following notations are used in Figs. 1 and 2: a (crack length), b (specimen width), L and $2L$ (span length), E_{11} (flexural modulus), E_{33} (through-thickness modulus), G_{13}, G_{23} (shear moduli in the x-z and y-z plane), ν_{13} (Poisson's ratio), $k=5/6$ (shear correction factor), c (uncracked length in the ONF and OLB specimens, $c=2L-a$) and s (the position of applied load in the ONF, OLB, 4ENF and MSCB specimens). Equations (6)–(20) take the linear elastic deformation effects into consideration. It is assumed that all of the utilized systems are linear elastic and nonlinear deformation does not take place. Referring to Fig. 1(a) the compliance of the mode-I DCB specimen is [10]:

$$C^{DCB} = \frac{8a^3}{2bh^3E_{11}} + \frac{2a^3}{bh^3E_{11}} \times \left[f_{W1} + \frac{f_{SV}}{2} + \frac{1}{k}\left(\frac{h}{a}\right)^2\left(\frac{E_{11}}{G_{13}}\right)\right]. \tag{6}$$

Figure 1(b-c-d) and (e) schematically represent the mode-II ENF [8], 4ENF [4], ELS [1, 2] and ONF [12] specimens. The compliances of these systems are [13, 20]:

$$C^{ENF} = \frac{3a^3 + 2L^3}{8bh^3E_{11}} + \frac{2L}{8bhkG_{13}} + \frac{a^3}{8bh^3E_{11}}f_{SH1}, \tag{7}$$

$$C^{4ENF} = \frac{(9a + 6L - 12s)s^2}{8bh^3E_{11}}, \tag{8}$$

where $s=(2L-d)/2$ [see Fig. 1(c)], furthermore:

$$C^{ELS} = \frac{3a^3 + L^3}{2bh^3E_{11}} + \frac{L}{2bhkG_{13}} + \frac{a^3}{2bh^3E_{11}}f_{SH1} + \frac{3}{\pi} \times \frac{L^2}{2bh^2E_{11}}\left(\frac{E_{11}}{G_{13}}\right)^{\frac{1}{2}}, \tag{9}$$

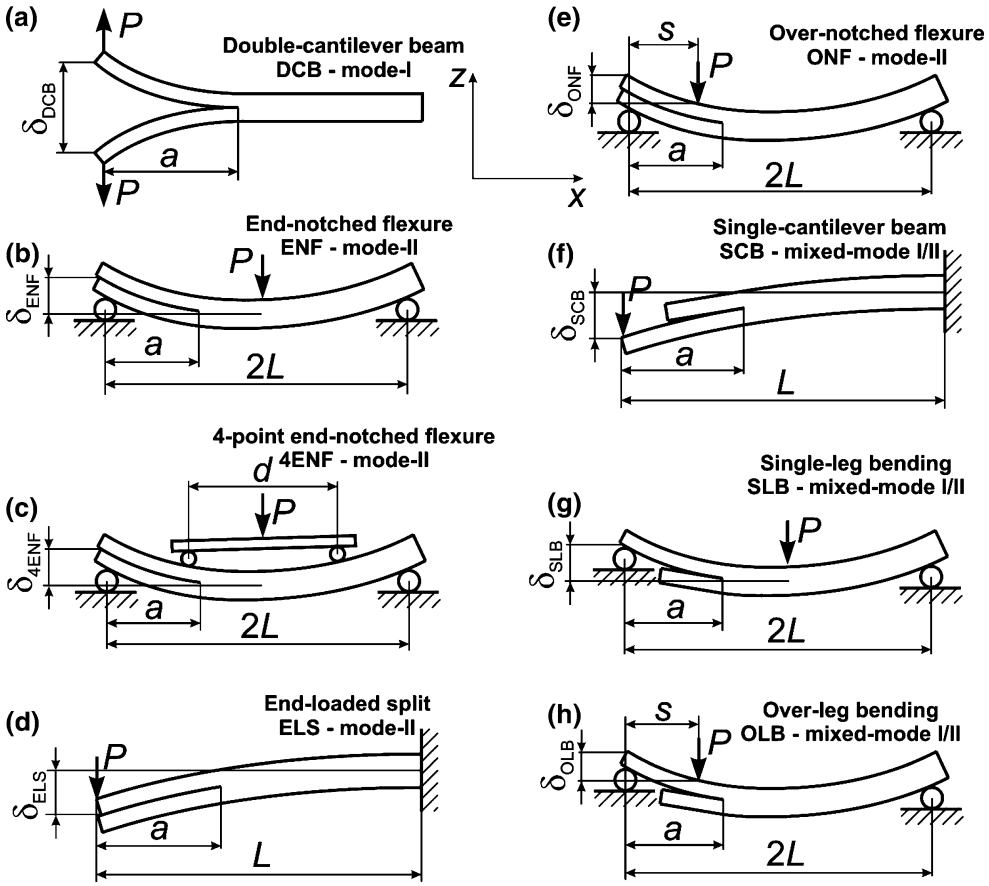

Fig. 1 Schematic illustration of the DCB, ENF, 4ENF, ELS, ONF, SCB, SLB and OLB composite fracture specimens

$$C^{ONF} = \frac{s^2c^3}{8bh^3E_{11}L^2} \times \left[1 + 4\frac{a}{c} + 8\frac{aL}{c^2} + 16\frac{aL^2}{c^3} + 8\frac{Ls(s-4L)}{c^3}\right] + \frac{s(2L-s)}{8bhkG_{13}L} + \frac{s^2c^3}{8bh^3E_{11}L^2}f^*_{SH1}. \tag{10}$$

In the sequel three mixed-mode I/II configurations are utilized, all of them produce an approximately constant mixed-mode ratio of G_I/G_{II}=1.33. Following the order of Fig. 1 (f, g and h), the compliances of the SCB [14, 15], SLB [16] and the OLB [17] specimens become:

$$C^{SCB} = \frac{7a^3 + L^3}{2bh^3E_{11}} + \frac{a+L}{2bhkG_{13}} + \frac{a^3}{2bh^3E_{11}} \times \left[f_{W1} + f_{SH1} + \frac{f_{SV}}{2}\right] + \frac{3}{\pi}\frac{L^2}{2bh^2E_{11}} \times \left(\frac{E_{11}}{G_{13}}\right)^{\frac{1}{2}}, \tag{11}$$

$$C^{SLB} = \frac{7a^3 + 2L^3}{8bh^3E_{11}} + \frac{a+2L}{8bhkG_{13}} + \frac{a^3}{8bh^3E_{11}} \times \left[f_{W1} + f_{SH1} + \frac{f_{SV}}{2}\right], \tag{12}$$

$$C^{OLB} = \frac{s^2c^3}{8bh^3E_{11}L^2}\left[1 + 8\frac{a}{c} + 16\frac{aL}{c^2} + 32\frac{aL^2}{c^3} + 16\frac{Ls(s-4L)}{c^3}\right] + \frac{s[4L(2L-s)-sc]}{8bhkG_{13}L^2} + + \frac{s^2c^3}{8bh^3E_{11}L^2}\left[f^*_{W1} + f^*_{SH1} + \frac{f^*_{SV}}{2}\right], \tag{13}$$

where the factors are:

$$f_{W1} = 5.07\left(\frac{h}{a}\right) \times \left(\frac{E_{11}}{E_{33}}\right)^{\frac{1}{4}} + 8.58\left(\frac{h}{a}\right)^2\left(\frac{E_{11}}{E_{33}}\right)^{\frac{1}{2}} + 2.08\left(\frac{h}{a}\right)^3\left(\frac{E_{11}}{E_{33}}\right)^{\frac{3}{4}}, \tag{14}$$

$$f_{SH1} = 0.98\left(\frac{h}{a}\right)\left(\frac{E_{11}}{G_{13}}\right)^{\frac{1}{2}} + 0.43\left(\frac{h}{a}\right)^2\left(\frac{E_{11}}{G_{13}}\right), \tag{15}$$

$$f_{SV} = \frac{12}{\pi}\left(\frac{h}{a}\right)\left(\frac{E_{11}}{G_{13}}\right)^{\frac{1}{2}},$$

furthermore in the ONF and OLB specimens (equations 10 and 13) the factors, $f_{W1}{}^*$, $f_{SV}{}^*$ and $f_{SH1}{}^*$ are:

$$f^*_{W1} = f_{W1}\big|_{a=c},\ f^*_{SV} = f_{SV}\big|_{a=c},\ f^*_{SH1} = f_{SH1}\big|_{a=c}, \tag{16}$$

where $c=2L-a$ is the length of the uncracked portion of the ONF and OLB specimens. Finally the compliance of the mixed-mode-II/III MSCB specimen in Fig. 2 is [19]:

$$C_{MSCB} = \frac{8a^3}{b^3 h E_{11}}[f_{EB1} + f_{TIM1} + f_{FT1} + f_{S-V1}], \tag{17}$$

where:

$$f_{EB1} = 1 - 6\left(\frac{s}{a}\right) + 12\left(\frac{s}{a}\right)^2 - 6\left(\frac{s}{a}\right)^3, \tag{18}$$

$$f_{TIM1} = 0.3\left(\frac{b}{a}\right)^2\left(\frac{E_{11}}{G_{13}}\right),$$

$$f_{FT1} = 0.19\frac{1}{\varsigma}\left(\frac{b}{a}\right)^2\left(\frac{E_{11}}{G_{12}}\right),\ \varsigma = 1 - 0.63\mu\frac{h}{b}, \tag{19}$$

$$\mu = \left(\frac{G_{13}}{G_{12}}\right)^{\frac{1}{2}},$$

$$f_{S-V1} = \left[0.48 - 1.91\left(\frac{s}{a}\right) + 1.91\left(\frac{s}{a}\right)^2\right]\left(\frac{b}{a}\right)\left(\frac{E_{11}}{G_{13}}\right)^{\frac{1}{2}}, \tag{20}$$

Equation (17) is based on the linear interpolation of δ_1 and δ_2, where δ_1 and δ_2 are the displacements of the MSCB specimen at rollers A and B (see Fig. 2), respectively. The half of crack tearing displacement (CTD) is denoted by $\delta/2$ calculated at roller C, which was directly measured by a dial gauge. The total CTD (δ) is measured through the displacement of the two grips (grip 1 and grip 2 in Fig. 2).

Application of the Traditional Criterion

The traditional criterion is given by equation (3) and equation (5). Substituting the above given compliances (equations (6)–(20)) into equation (5) the stability of the system can be represented as a function of the normalized crack length, a/L and a/a_0. The solution of equations (3) and (5) for the specimens demonstrated in Fig. 1 is depicted in Fig. 3(a–c). Namely, Fig. 3(a) plots the results of the DCB, ELS and SCB specimens. The reason for this classification is that these coupons are loaded at the end,

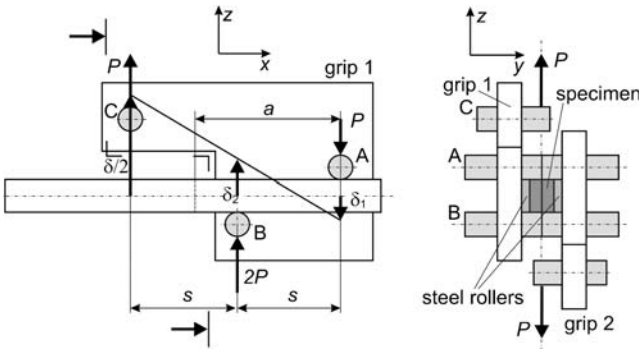

Fig. 2 Schematic illustration of the MSCB specimen

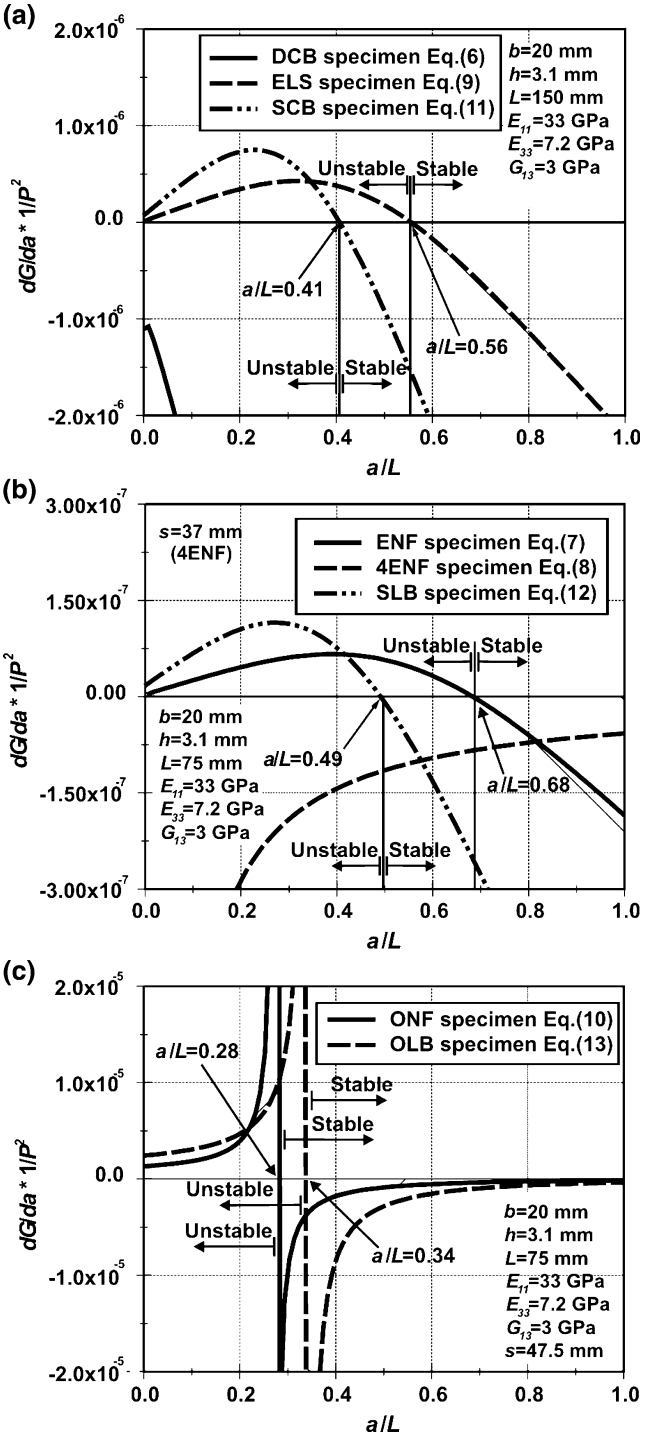

Fig. 3 Crack stability chart of the DCB, ELS, SCB (**a**), ENF, 4ENF, SLB (**b**), and ONF, OLB **c** specimens in accordance with the traditional criterion

they can be investigated in the same crack length range and finally, the specimens exhibit very similar fracture behavior. Running through the results it is seen that there is no stability problem in the DCB specimen, while the restrictions in the ELS and SCB specimens are: $a \geq 0.56L$ and $a \geq 0.41L$, respectively.

In Fig. 3(b) the results for the ENF, 4ENF and the SLB systems are classified. Similarly to Fig. 3(a), these systems can be investigated in the same crack length range. The 4ENF test promotes always stable crack propagation (it has been highlighted by others, e.g. in [4]), on the other hand the chosen crack length of the ENF and SLB specimens must satisfy the requirements of $a \geq 0.68L$ and $a \geq 0.49L$, respectively. Finally, the stability chart of the ONF and OLB specimens are shown in Fig. 3(c). Although mathematically there is a restriction for both cases, physically "*a*" should always be higher than "*s*" (the position of the applied load from the left specimen end, refer to Fig. 1(e and h)), which—under the present geometrical parameters (s=47.5 mm, L=75 mm)—involves that $a \geq 0.63L$ for both systems, i.e. it invokes a strongest restriction than those in Fig. 3(c).

The stability chart of the MSCB specimen is shown in Fig. 4 including four different values of "*s*" (refer to Fig. 2). Note that *s* is not the same as in Fig. 1(e and h). It is seen in Fig. 4 that when s=26 mm then the stable ranges are $a \geq$ 74.3 mm and $a \leq$48.3 mm, i.e. if a_0=150 mm, then: $a/a_0 \geq$ 0.49 and $a/a_0 \leq 0.32$ for stable crack propagation in the MSCB specimen.

As a summary of the results it seems that the application of this criterion is quite simple. However, when there is no analytical solution, then the $C(a)$ function should be determined by experimental measurements and then a proper curve-fit technique is necessary. The relevant method is called as compliance calibration (CC) [1–4, 6],

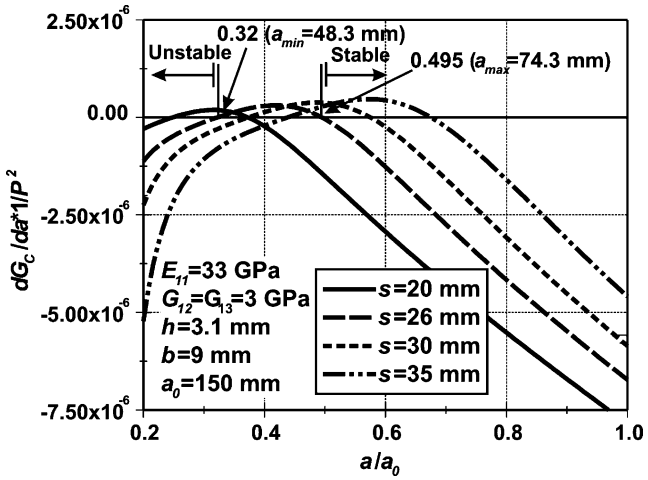

Fig. 4 Crack stability chart of the MSCB specimen in Fig. 2 in accordance with the traditional criterion

which is the most accurate data reduction technique in fracture toughness measurements under mode-I, mode II and mixed-mode I/II conditions. The drawback of the method is that its accuracy depends upon the number of points used for the curve-fit process. Further complications take place if the compliance of the system is relatively small, leading to the large scatter of the measured data. In this case we can make significant mistakes due to the smoothing that comes into play by the curve-fitting, some relevant examples are the mode-III crack rail shear (CRS) specimen [21] and also the MSCB specimen [18]. It should be mentioned that although in this case the compliance vs. crack length relationship may be obtained by finite element calculations, it requires the precise determination of the material properties (elastic moduli and Poisson's ratios) of the material. This issue is relatively simple when the bending dominates the deformation; however when the shape of the specimen strongly differs from a slender beam, then shearing, transverse deformation and Poisson's effect may contribute significantly to the deformation process. The additional material properties (G_{12}, G_{13}, G_{23}, ν_{12}, ν_{13}, ν_{23}, E_{22} and E_{33}) can be approximated by rule of mixtures, or—utilizing different tests—experimental measurements. It should be emphasized that the additional material properties can only be determined approximately and in some cases (for example in short fiber-reinforced or angle-ply laminated composites) they are highly questionable. In such cases due to the large number of measurement and specimen types required for testing it is worth the effort to use an experimental establishment of the crack stability limits, especially when it leads to the same limits as the traditional criterion. To this end in the followings we verify the traditional criterion by experimental observations.

Verification of the Traditional Criterion

To verify the traditional crack stability criterion a large amount of experiments were performed on the configurations shown in Figs. 1–2.

Experimental Work

Specimen preparation

The constituent materials of the E-glass/polyester composite were procured from Novia Ltd. The properties of the E-glass fiber are E=70 GPa and ν=0.27, while for the unsaturated polyester resin the elastic properties are E= 3.5 GPa and ν=0.35. Both were considered to be isotropic. The unidirectional ($[0°]_{14}$) E-glass/polyester specimens with nominal thickness of $2h$=6.2 mm, width of b= 20 mm (except for the MSCB specimen where b=9 mm

was applied), and fiber-volume fraction of V_f=43% were manufactured in a special pressure tool. A polyamide (PA) insert with thickness of 0.03 mm was placed at the midplane of the specimens to make an artificial starting defect. A significant advantage of the E-glass/polyester material used in this study is its transparency, which allows for the visual observation of crack initiation/propagation. The tool was left at room temperature until the specimens became dry. Then the specimens were removed from the tool and were further left at room temperature for 4–6 h. At the final stage the specimens were cut to the desired length and were precracked in opening mode of 4–5 mm by using a sharp blade. The reason for that was in this case it was possible to make a straight crack front, which is important in the case of the crack length measurement and the observation of crack initiation.

Material properties, specimen dimensions

The flexural modulus was determined from a three-point bending test with span length of $2L$=150 mm using six uncracked specimens with $2h$=6.2 mm (height) and b=20 mm (width). The experiments resulted in E_{11}=33 GPa. The additional properties were predicted from simple rules of mixture, in this way E_{33}=7.2 GPa, G_{13}= G_{23}=3 GPa and ν_{13}=0.27 were obtained.

Crack initiation tests

In all the presented cases the fracture behavior of the systems were investigated in extended crack length ranges. The specimen dimensions were $2h$=6.2 mm, b=20 mm, and the whole length of the specimens was 180 mm. At each crack length only one specimen was used and was loaded up to fracture initiation. The applied load was measured by using an Amsler testing machine (manufactured in Switzerland), while the displacement of the specimen was recorded by a mechanical dial gauge. In the followings the performed tests are detailed.

In the DCB test [Fig. 1(a)] steel hinges were bonded to the specimen faces. The DCB specimens were prepared with the following crack lengths: a=25, 30, 35, 40, 45, 50, 55, 60, 65, 70, 75, 80, 90, 100, 110, 120, 130, 140 and 150 mm.

For the ENF test [Fig. 1(b)] eleven specimens were used to test the material in the range of a=25 to 75 mm with 5 mm increments. The specimens were put into a three-point bending setup, the method of the load and displacement measurement was the same as that of the DCB specimen. The span length was $2L$=150 mm.

In the case of the 4ENF [Fig. 1(c)] coupon the investigated crack length range was: a=45 to 105 mm with 5 mm increments. The specimens were loaded through a steel block, which divided the applied load into two equal parts inducing pure bending in the central region of the specimen. Load and displacement recordings were also performed. The span length was $2L$=150 mm, the distance between the loading rollers was d=76 mm.

The mode-II ELS [Fig. 1(d)] test was performed using specimens with a=35, 40, 45, 50, 55, 60, 65, 70, 75, 80, 90, 100, 110, 120, 130 and 140 mm. The coupons were put into a clamping fixture and were loaded at the end. The distance from the load application and the clamped end was L=150 mm. The load and displacement was recorded until crack initiation.

For the ONF [Fig. 1(e)] test the range of a=50 to 105 mm with 5 mm increments was covered. The specimens were loaded excentrically to the vertical centerline of the system, the distance from the left specimen side was s=47.5 mm, the span length was $2L$=150 mm.

The mixed-mode I/II SLB [Fig. 1(g)] test was performed in the range a=20 to 75 mm with 5 mm increments under the same geometrical parameters as in the ENF test.

The crack lengths of the tested SCB specimens [Fig. 1(f)] were: a=20, 25, 30, 35, 40, 45, 50, 55, 60, 65, 70, 75, 80, 90, 100, 110, 120, 130 and 140 mm under the same conditions as in the ELS specimen.

The OLB specimens [Fig. 1(h)] including crack lengths in the range of a=50 to 115 mm with 5 mm increments were prepared. The geometry of the system corresponded to that of the ONF test.

Finally, in the MSCB system (Fig. 2) thirteen specimens were used with the crack lengths of a=45 to 105 mm with 5 mm increments, at each crack length four specimens were tested.

Experimental Results

The most important conclusion of this part is based on an experimental observation. In some of the investigated systems it was observed that it was not possible to investigate the crack propagation if the crack length of interest was lower than a certain value, i.e. the stability of the system was restricted by the crack length/span length ratio. Figure 5 shows the case of the SCB specimen as an example, where Fig. 5(a) shows the specimen with relatively small crack length under initial loading and Fig. 5(b) indicates the sudden crack jump (approximately 60 mm crack increment). The elapsed time between the states of Fig. 3(a and b) is only a few tenths of a second. In all the investigated cases, if instability was observed then the fact of the instability was represented by a sudden crack jump (similarly to that demonstrated in Fig. 5), which prevented the measurement of the crack length and load values, actually the systems became unstable. The point of instability (if instability took place) was always at that point, where the critical displacement reached its minimum

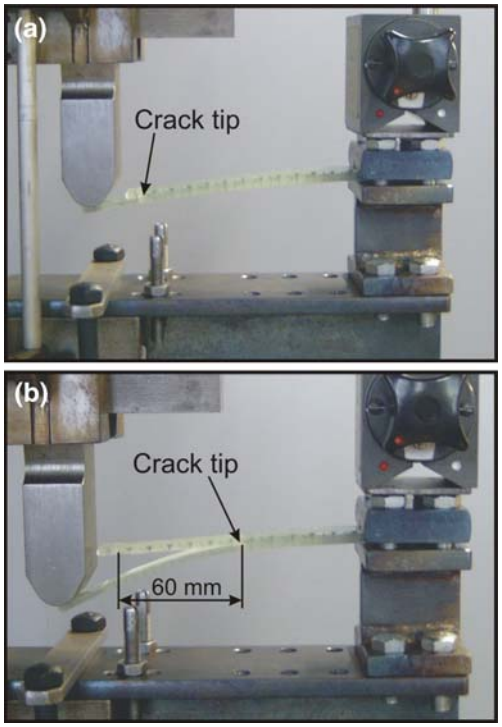

Fig. 5 Crack jump in the SCB specimen

value in the relevant crack length range. In accordance with experimental observations the stability is determined by the condition:

$$\frac{d\delta_C(a)}{da} \geq 0, \tag{21}$$

i.e. the stability of crack propagation is determined by the derivative of the critical displacement with respect to the crack length. The critical displacement is considered to be the value of the specimen displacement at the point of load application at crack initiation. In the case of the DCB specimen the critical displacement is equivalent to the crack opening displacement (COD) [7]. In accordance with the COD theorem the crack opening displacement governs the crack extension [11]. However in all of the other cases there is no relationship between the COD and the critical displacement, by the way the COD theorem is essentially related to mode-I problems.

The results are presented in Figs. 6–8(a) and in each case there are two curves denoted by "experiment (1)" and "analysis (2)". The notation "experiment (1)" means that the displacement values were measured experimentally by a dial gauge. On the other hand the "analysis (2)" means that the critical force (P_C) at crack initiation was measured and the critical displacement was calculated by the analytical model using equation (6)–(20) utilizing the relationship of $C=\delta/P$.

Figure 6(a) represents the critical displacement values measured from the DCB, ELS and SCB tests as the function of the crack length. The measured displacement values were fitted by a second, third or fourth order polynomial as the function of the crack length and the point where the derivative of the curve was horizontal was believed to be the limit value regarding the stability of the system. The experimental observations confirmed this stability limit. Even the analytical solution is given in Fig. 6(a), indicating a very good agreement with the experimentally measured points. Figure 6(b) shows the crack stability chart calculated by using equation (21), where the limit ratios (a/L) are also highlighted. The values in the parentheses were obtained from the analytical solutions. The stability limit for the DCB specimen is the result of the curve fitting of the critical displacement values, i.e. the derivative of the fitted curve changes its sign if $a/L=0.043$, although this is not shown in Fig. 6(a). On the other hand the fitted curve is valid only between the first and last measured points. In a similar fashion Fig. 7(a–b) plot the same results for the ENF, 4ENF and SLB configurations. The only difference is that in the case of

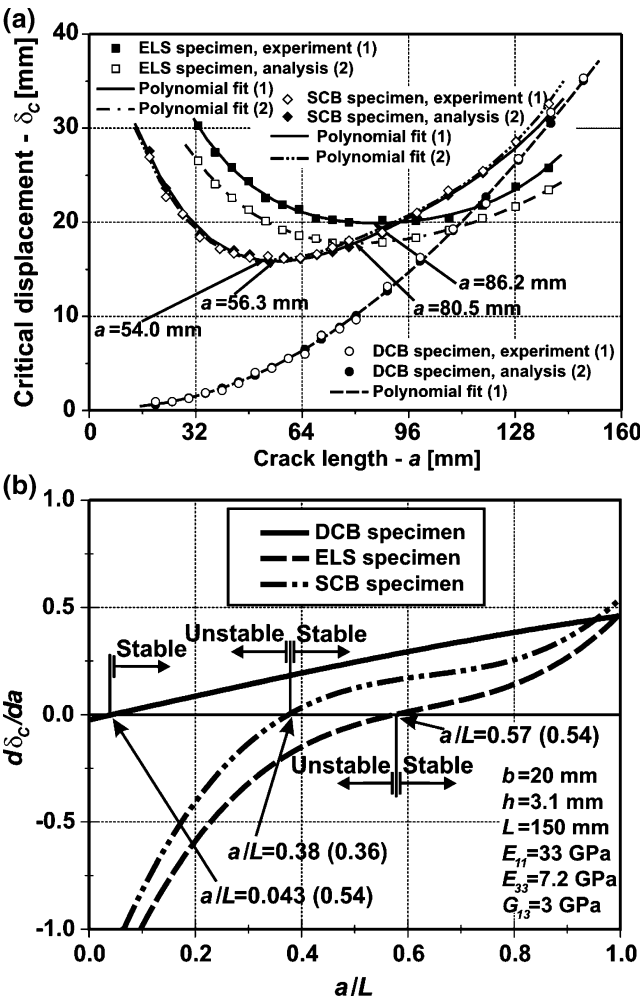

Fig. 6 The experimentally measured critical displacements (**a**) and the crack stability chart of the DCB, ELS and SCB specimens (**b**) (the stability limits in the parentheses were obtained from analysis (2))

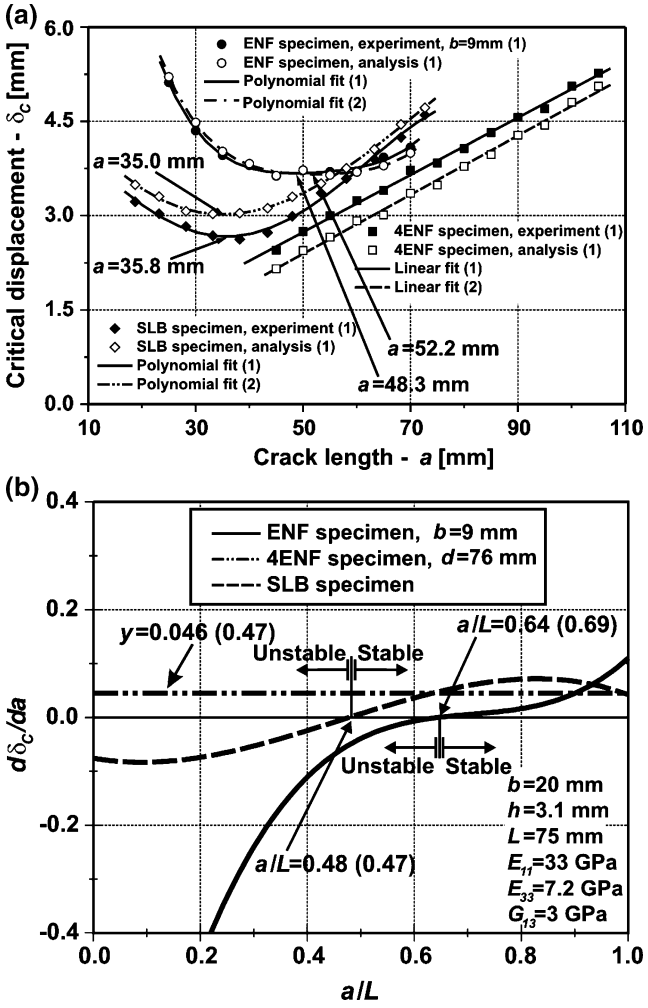

Fig. 7 The experimentally measured critical displacements (**a**) and the crack stability chart of the ENF, 4ENF and SLB specimens (**b**) (the stability limits in the parentheses were obtained from analysis (2))

the 4ENF system a linear fit was made. For the ONF and OLB specimens the experimental results and the stability diagrams are demonstrated in Fig. 8(a–b). Finally Fig. 9 shows the critical displacements as the function of the crack length in the MSCB specimen, the fitted curve and the crack length, where the derivative of the fitted curve is zero.

Comparison

Considering the results of the traditional stability criterion and the experimental observations the following conclusions may be drawn. In those cases, where instability takes place the traditional criterion and the experiment agrees excellently, this can be justified by the limit values of a/L in Table 1. The traditional criterion shows that for the ELS and SCB specimens the limit is a/L=0.56 and a/L=0.41 [Fig. 3(a)], respectively while based on the experimental observations the limits are a/L=0.57 and a/L=0.38 [Fig. 5(b)], for the same systems, respectively. The difference is−1.8% in the former and +7.3% in the latter case. Both the traditional criterion and the experiment indicate stable crack propagation for the DCB specimen. For the ENF and SLB test the same results are: a/L=0.68 and a/L=0.64 (+6%), a/L=0.49 and a/L=0.48 (+2%), respectively. The crack propagation is always stable in the 4ENF specimen, as it was confirmed by both the criterion and the experimental observation. For the ONF and OLB specimen there are no stability problems in accordance with both the criterion and the experimental observation. Finally for the MSCB specimen the analysis provides an unstable range between 48.3 mm≤a≤72.3 mm, while the experiments indicate only a transition at a= 72.46 mm. It involves an extremely small difference compared to the upper limit of the unstable zone.

So it seems that the experimental observations show excellent agreement with the results of the traditional stability criterion in all the cases presented (except for the MSCB specimen, where it does not predict the lower range of the unstable zone). Therefore the traditional criterion was

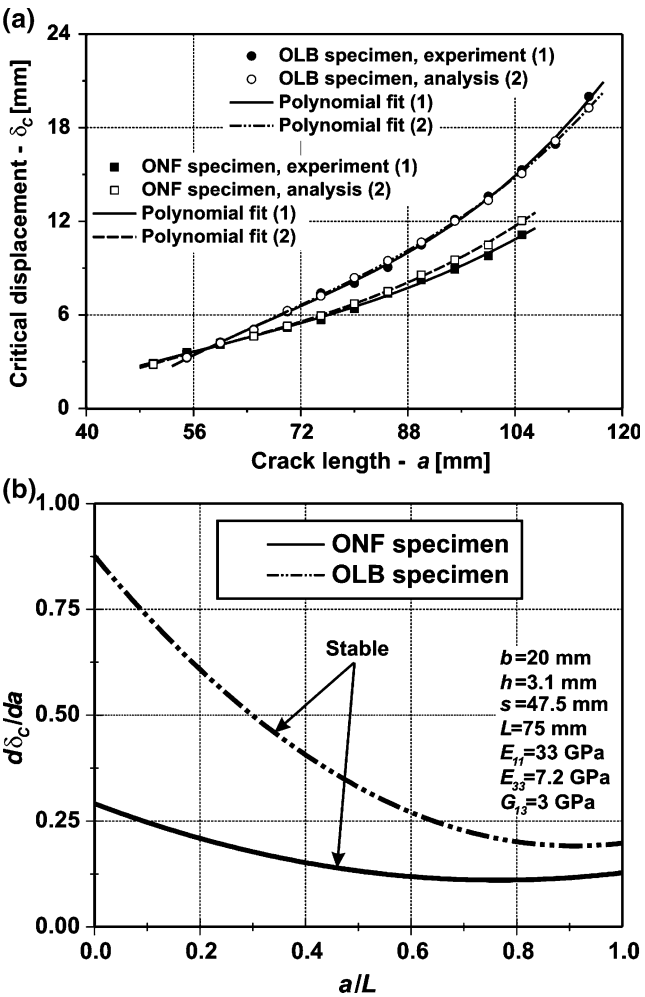

Fig. 8 The experimentally measured critical displacements (**a**) and the crack stability chart of the ONF and OLB specimens (**b**)

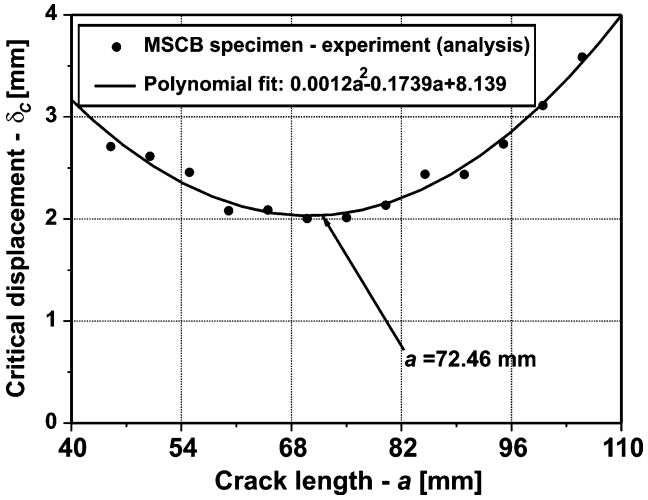

Fig. 9 The experimentally measured critical displacements of the MSCB specimen

verified and it may be assumed that the agreement would be similar in other type of fracture mechanical configurations, and consequently equation (21) can be used as an alternative of equation (3).

In the following the advantages and drawbacks of the experimental establishment of the stability limit over the traditional criterion are highlighted. First of all the traditional criterion requires the determination of the compliance-crack length relation, either analytically, numerically or experimentally. The first method can be applied only if the system behaves as a slender beam, or it is a plate. The numerical and analytical calculation requires the accurate determination of the material properties. This is especially difficult if the tested material is strongly anisotropic. As regarding to the experimental compliance measurement it is a possible case that the compliance of the system is relatively small, which can lead to significant deviation of the data and serious errors in the curve-fit process and the derivative of the compliance curve, and so the limit value of the ratio a/L would be determined erroneously.

In contrast, for the experimental observation it is not required to determine the material properties. However in systems with relatively small compliance (displacement) values the method can give misleading results. It should be mentioned that the identification of the limit ratio of stability is possible even in those cases where the experimental error is relatively huge. Displaying the measured critical displacement values as the function of the crack length it is possible to identify approximately the minimum value (which theoretically corresponds to the limit of stability) in accordance with equation (21).

It is also true that one should perform the crack initiation tests to determine the stability range. On the one hand, this can be done by using one specimen with relatively long crack length and shifting the specimen in the fixture (ENF, ELS, SLB and SCB tests). If the crack length of the specimen is in the unstable range then due to the sudden crack jump demonstrated in Fig. 5 the specimen will not be utilizable once again. It is more reasonable to determine the stability limit using one specimen (and by shifting in the fixture) than to find out the stability limit by a "try-out" method abusing several specimens.

Conclusions

In this work the traditional crack stability criterion was established by experimental observations. Several fracture mechanical systems including mode-I, mode-II, mixed-mode I/II and mixed-mode II/III configurations were tested experimentally and based on an observation it was found that the stability of the system depends on the derivative of the critical displacement (displacement at crack initiation) of the specimens at the point of load application.

The results obtained from experimental observations were compared to those by the traditional criterion of crack stability. The criterion and the experiments agreed very well considering the limit ratios (a/L) of the stability, and corresponded even in those cases when there was no

Table 1 The limit ratios of the crack stability in accordance with the traditional crack stability criterion and experimental observations

Configuration	Traditional criterion a/L—limit ratio of stability	Experimental observation a/L—limit ratio of stability	Difference [%]
DCB	–	0.043	–
ENF	0.68	0.64	5.88
4ENF	–	–	–
ELS	0.56	0.57	−1.78
ONF	–	–	–
SCB	0.41	0.38	7.32
SLB	0.49	0.48	2.05
OLB	–	–	–
MSCB	0.32, 0.495	0.48	−, 3.03

stability problem. Based on the experimental results a simple condition including the critical displacement of the specimens was formulated as an alternative of the traditional criterion. It is a reasonable assumption that the condition based on experimental observations is applicable to other types of materials and even to different fracture mechanical systems. In some cases—for example when the material is anisotropic and we do not know the material properties with sufficient accuracy or the compliance of the system is difficult to measure precisely—the condition based on experimental observations is more reasonable to apply than the traditional crack stability criterion.

Acknowledgements This research work was supported by the János Bolyai Research Scholarship of the Hungarian Academy of Sciences and by the Hungarian National Research Fund (OTKA) under Grant No. 34040. The author is grateful to his father (András L. Szekrényes) for the construction of the experimental equipments.

References

1. Hashemi S (1990) J, Kinloch and JG. Williams. The effects of geometry, rate and temperature on mode I, mode II and mixed-mode I/II interlaminar fracture toughness of carbon fibre/poly (ether-ether ketone) composites. J Compos Mater 24:918–956. doi:10.1177/002199839002400902
2. Hashemi S (1990) J, Kinloch and JG. Williams. Mechanics and mechanisms of delamination in a poly(ether sulphone)-fibre composite. Compos Sci Technol 37:429–462. doi:10.1016/0266-3538(90)90013-U
3. Schön J, Nyman T, Blom A, Ansell H (2000) Numerical and experimental investigation of a composite ENF-specimen. Eng Fract Mech 65:405–433. doi:10.1016/S0013-7944(99)00137-X
4. Schuecker C, Davidson BD (2000) Evaluation of the accuracy of the four-point bend end-notched flexure test for mode II delamination toughness determination. Compos Sci Technol 60:2137–2146. doi:10.1016/S0266-3538(00)00113-5
5. Crews JH Jr, Reeder JR (1988) A mixed-mode bending apparatus for delamination testing. NASA Technical Memorandum 100662, August, 1–37.
6. Reeder JR, Crews JH Jr (1990) Mixed-mode bending method for delamination testing. AIAA J 28:1270–1276. doi:10.2514/3.25204
7. Olsson R (1992) A simplified improved beam analysis of the DCB specimen. Compos Sci Technol 43:329–338. doi:10.1016/0266-3538(92)90056-9
8. Carlsson LA, Gillespie JW, Pipes RB (1986) On the analysis and design of the end notched flexure (ENF) specimen for mode II testing. J Compos Mater 20:594–604. doi:10.1177/002199838602000606
9. Kim BW, Mayer AH (2003) Influence of fiber direction and mixed-mode ratio on delamination fracture toughness of carbon/epoxy laminates. Compos Sci Technol 63:695–713. doi:10.1016/S0266-3538(02)00258-0
10. Anderson, TL (2005) Fracture Mechanics—Fundamentals and Applications 3rd edn. CRC, Taylor & Francis Group, Boca Raton, London, New York, Singapore.
11. Kanninen MF, Popelar, CH (1985) Advanced Fracture Mechanics. Oxford University Press, New York
12. Wang W-X, Takao Y, Nakata, M (2003) Effects of friction on the measurement of the mode II interlaminar fracture toughness of composite laminates. Proceedings of the 14th International Conference on Composite Materials, San Diego, California, USA, July 14–18.
13. Szekrényes A (2005) Mode-II fracture in E-glass-polyester composite. J Compos Mater 39(19):1747–1768. doi:10.1177/0021998305051120
14. Blanco N, Gamstedt EK, Costa J, Trias D (2006) Analysis of the mixed-mode end load split delamination test. Compos Struct 76:14–20. doi:10.1016/j.compstruct.2006.06.003
15. Reyes G, Cantwell WJ (2000) The mechanical properties of fibre-metal laminates based on glass fibre reinforced polypropylene. Compos Sci Technol 60:1085–1094. doi:10.1016/S0266-3538(00)00002-6
16. Davidson BD, Sundararaman V (1996) A single leg bending test for interfacial fracture toughness determination. Int J Fract 78:193–210. doi:10.1007/BF00034525
17. Szekrényes A, Uj J (2007) Over-leg bending test for mixed-mode I/II interlaminar fracture in composite laminates. Int J Damage Mech 16(1):5–33. doi:10.1177/1056789507060774
18. Sharif F, Kortschot MT, Martin RH (1995) Mode III delamination using a split cantilever beam. In: Martin RH (ed) Composite materials: Fatigue and fracture—Fifth Volume ASTM STP 1230. ASTM, Philadelphia, pp 85–99
19. Szekrényes A (2007) Delamination fracture analysis in the G_{II}-G_{III} plane using prestressed transparent composite beams. Int J Solids Struct 44:3359–3378. doi:10.1016/j.ijsolstr.2006.09.029
20. Szekrényes A (2007) Improved analysis of unidirectional composite delamination specimens. Mech Mater 39:953–974. doi:10.1016/j.mechmat.2007.04.002
21. Becht G, Gillespie JW Jr (1988) Design and analysis of the crack rail shear specimen for mode III interlaminar fracture. Compos Sci Technol 31:143–157. doi:10.1016/0266-3538(88)90088-7